Available online at www.sciencedirect.com

jmr&t Journal of Materials Research and Technology

journal homepage: www.elsevier.com/locate/jmrt

Original Article

Strain hardening behavior and microstructure evolution of gradient-structured Cu-Al alloys with low stack fault energy

Huan Liu [a], *Bo Gao* [b], *Yi Yang* [a], *Mengning Xu* [b], *Xingfu Li* [a], *Cong Li* [a], *Hongjiang Pan* [a], *Jingran Yang* [c], *Hao Zhou* [b,**], *Xinkun Zhu* [a,*], *Yuntian Zhu* [b,d]

[a] *Faculty of Materials Science and Engineering, Kunming University of Science and Technology, Kunming 650093, China*

[b] *Nano and Heterogeneous Materials Center, School of Materials Science and Engineering, Nanjing University of Science and Technology, Nanjing 210094, China*

[c] *City College, Kunming University of Science and Technology, Kunming, Yunnan, 650051, China*

[d] *Department of Materials Science and Engineering, City University of Hong Kong, Hong Kong 999077, China*

ARTICLE INFO

Article history:
Received 8 February 2022
Accepted 2 May 2022
Available online 13 May 2022

Keywords:
Heterostructured materials
Cu alloys
Stacking fault energy
Gradient structure
Deformation twinning
HDI hardening

ABSTRACT

Nanocrystallization can significantly improve the strength and hardness of metallic materials, but usually sacrifice ductility due to low work hardening capability. Heterostructured materials are an emerging class of materials with superior performances, because of their outstanding work hardening capability. In this work, a type of heterostructured material, a gradient structured Cu-Al alloy, was produced by surface mechanical attrition treatment (SMAT) at liquid nitrogen temperature. After SMAT processing, the yield strength was increased to more than 1.5 times, and the ductility remained almost unchanged. In conjunction with hetero-deformation induced (HDI) hardening, stacking fault energy is another important factor to increase the strain hardening in the system. Low stacking fault energy increased the density of stacking fault, and led to a finer spacing of nano twins (~5.4 nm) and higher dislocation storage (8×10^{13} m^{-2}) in the SMATed Cu-Al alloy at the intermediate strain stage. A significant up-turn of strain-hardening rate was also induced by low stacking fault energy.

1. Introduction

Materials with high strength and ductility are desired for many industrial applications. Nano-grained materials usually show outstanding strength and hardness, while their ductility is limited because of the poor work hardening ability [1–3]. In the past decades, numerous researchers explored efficient approaches to improve the combination of strength and ductility [4,5]. The gradient-structured materials have been

* Corresponding author.
** Corresponding author.
E-mail addresses: hzhou511@njust.edu.cn (H. Zhou), xk_zhu@hotmail.com (X. Zhu).

https://doi.org/10.1016/j.jmrt.2022.05.027

proposed to enhance the yield strength and maintain considerable ductility [5–10]. Lu [11] introduced nano gradient-structural Cu rods by surface mechanical grinding treatment (SMGT), which nearly doubled the yield strength of coarse-grained sample. Additionally, the uniform elongation of the nano gradient structured Cu was almost the same as that of the coarse-grained sample. Gradient nanostructure is a typical heterostructure material (HSM) [12–14]. HSMs are usually composed of heterogeneous zones with dramatically different constitutive properties [7,15–17]. It has been demonstrated that the superior mechanical properties are mainly attributed to the significant interactions between the hetero-zones during deformation, which is related to the strain gradient, geometrically necessary dislocations (GNDs) pileups near the zone boundaries and the resulting hetero-deformation induced (HDI) hardening [18,19]. The additional HDI hardening helps with improving both the strength and ductility [16,20,21].

For face-centered cubic (FCC) materials, such as Cu alloys, the stacking fault energy (SFE) is another important factor that affects the mechanical properties. Instead of perfect dislocations, stacking faults (SFs) and nano twins (NTs) usually form in the alloys with low SFE. It has been demonstrated that high strain rate and low deformation temperature introduced more NTs formed during deformation. Recent studies showed that the FCC alloys with low SFE exhibited a high strain hardening rate and a good combination of strength and ductility, due to the influence of SFs and twins [5,22–28]. Similar to HSMs, the ductility of low SFE alloys were also affected by the high strain-hardening in the system [29–33]. Thus, it is worthy to explore the effect of SFE on plastic deformation in HSMs.

In the present study, we selected two typical Cu-Al alloys with different SFEs, namely the Cu-4.5 wt.% Al (SFEs: 12 mJ/m^2) and the Cu-6.9 wt.% Al (SFEs: 5 mJ/m^2) reported in Ref. [34]. All the samples were deformed by SMAT under liquid nitrogen temperature for 2 min to produce a gradient structured (GS) layer on the surface of CG sheet. To clarify the hardening behavior in different plastic deformation stages, microstructure evolution from the surface layer to center was characterized by EBSD and TEM. Furthermore, the microstructural evolution of the gradient layer at tensile strains of 0–0.22 was systematically investigated. It is found that Low stacking fault energy leads to significant up-turn of strain-hardening during deformation. Finer spacing of nano twins and higher dislocation storage is achieved in the Cu-Al alloy with lower SFE, corresponding to the hardening behavior under the corresponding strain.

2. Experimental procedures

Commercial binary Cu-Al alloys with Al contents of 4.5 and 6.9 wt.%, prepared from high purity components (99.95 wt.% Cu and 99.99 wt.% Al) by vacuum induction furnace, were investigated in this work, respectively. The cast ingots were rolled and machined into sheets with dimension of 100 × 50 × 4 mm^3. A vacuum annealing was operated at 923 K for 2 h to obtain a homogeneous coarse-grained microstructure. The surface mechanical attrition treatment (SMAT) processing was carried out at liquid nitrogen temperature. Before the SMAT deformation, two hundred stainless steel balls with a diameter of 8 mm were placed into the chamber of the SMAT machine. The vibration frequency of the SMAT machine was set as 50Hz. More detailed setting information of SMAT can be referred to Ref. [11]. Both the surfaces of samples were SMAT processed for 2 min to produce a gradient microstructure.

Uniaxial tensile tests were performed on a SHIMADZU Universal Tester, using dog-bone shaped samples with a gage length of 15 mm and a transverse section of 4 × 5 mm^2. The samples for tensile testing were cut for the SMAT deformed sheets having a thickness of 4 mm. As shown in Fig. 3a, the upper and lower surfaces (colored in blue) are the treated surfaces of SMAT. The uniaxial tensile tests and stress relaxation tests were performed at a strain rate of 5 × 10^{-4} s^{-1} at room temperature. To ensure the repeatability and accuracy of testing, at least 3 samples in each condition were performed. Micro-hardness measurements were carried out with a load of 25 g for a loading time of 15 s, and the average value was obtained at least at 3 points at the same depth. The stress relaxation test was loaded at a strain rate of 5 × 10^{-4} s^{-1} to a certain strain state with a stroke holding for 50s, then was reloaded at the same strain rate to the stress value. The combination of loading and holding at this time is a small

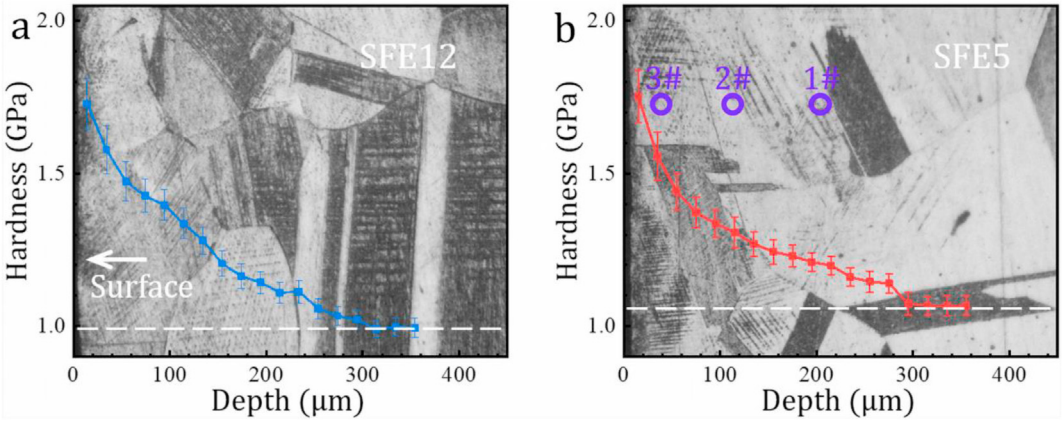

Fig. 1 – Optical micrography overlapped with distribution of microhardness nearby the surface. (a) Cu-4.5wt% Al (SFE12) alloy; (b) Cu-6.9wt% Al (SFE5).

cycle, each large cycle consists of 5 small cycles. And each sample performed at least 5 similar strain stage as a reference for relative comparison.

The cross-sectional samples were primary polished using sandpapers until 5000#, then polished by silicon dioxide polishing solution with 50 nm-scale, and finally removed the mechanically damaged layers by ionic polishing. The samples were observed on a field emission scanning electron microscope (FE-SEM, NOVA Nano SEM 450, 250 KV) equipped with an EBSD detector for the microstructure of the Cu-Al alloys with the different strain states, i.e., the strains of 0, 0.05, and 0.22. The distribution of geometrically necessary dislocations of the gradient structural Cu-Al samples were quantitated using the Channel-5 software. TEM observations were conducted on a JEM-2100 Plus transmission electron microscope operated at 200 kV. The specimens were cut from the cross-section direction of the sheets, and gently polished to a thickness of ~80 μm. A twin-jet electrolytic polishing was operated at 11.5 V and 23°C. The electrolyte for electrolytic polishing was 5 vol% C_2H_5OH, 25 vol% H_3PO_4 and 50 vol% H_2O. Samples for ion milling were performed at 5 keV and 8° for 2 h first, then were perforated at 4 keV and 5°. The broaden of the observation area is carried out with a milling voltage and angle of 2.5 keV and 3° for 2 h.

3. Results and discussion

We performed SMAT processing on two typical Cu-Al alloys with very low stacking fault energies, i.e. Cu-4.5wt.% Al (SFE: 12 mJ/m^2) and Cu-6.9wt.% Al (SFE: 5 mJ/m^2) [34], which will be hereafter referred to as SFE12 and SFE5 alloys, respectively. As shown in Fig. 1, gradient structure is formed in both-surface of the alloys, leading to a gradient distribution of microhardness from surface to center of the samples. Fig. 1 (a) and (b) show optical micrographs overlapped with the curves of hardness distribution of cross-sectional SFE12 and SFE5 samples, respectively. It is found that the hardness of the surface layer is significantly increased in both the samples, which is resulted from gradually decreasing strain rate with the depth.

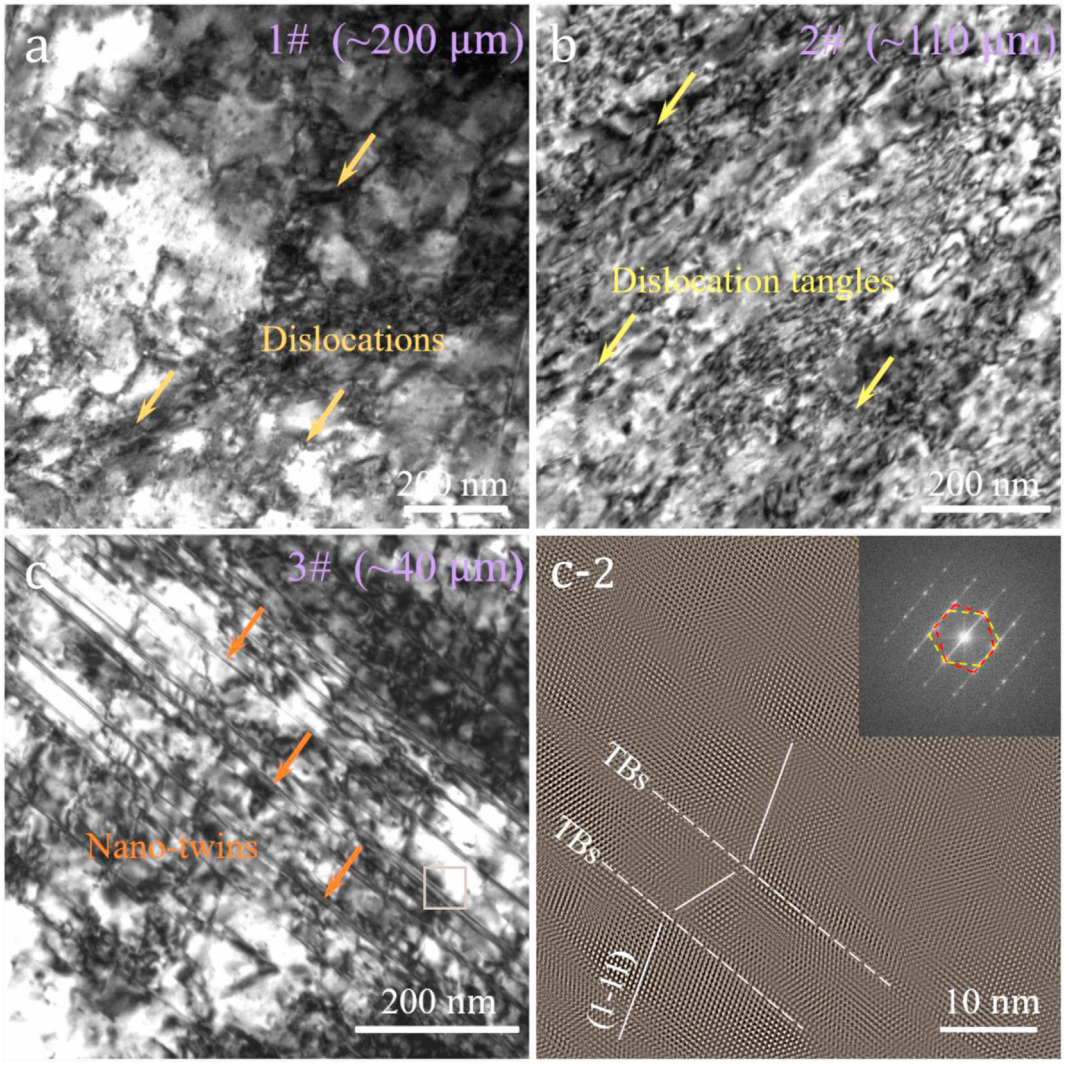

Fig. 2 – TEM images of the SFE5 sample at different depth. (a), (b) and (c-1) bright field TEM images at positions 1# (~200 μm), 2# (~110 μm) and 3#(~40 μm); (c-2) close-up high-resolution TEM image showing a nano-twin at the brown box in (c-1).

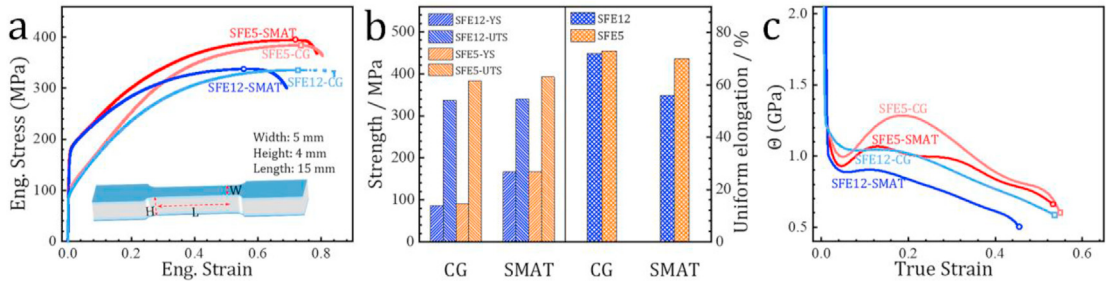

Fig. 3 – The tensile properties of SFE12 and SFE5 samples before and after SMAT processing. (a) engineering stress-strain curves, (b) histogram of yield strength, ultimate strength and uniform elongation, (c) strain hardening rate vs. true strain.

A rapid reduction of hardness is found in the depth from 10 (~1.7 GPa) to 200 (~1.2 GPa) μm. However, the microstructure observed by optical micrography is not clear enough to explain the underlying mechanism of the strength nearby the surface. We performed TEM characterizations on the positions 1#, 2# and 3# of the SFE5 sample to show more detailed microstructure (Fig. 1b).

Based on the distribution of microhardness, three typical positions at the depths of 200, 110 and 40 μm, are selected for TEM observations. It is found that the depth of 200 μm reaches the limit of SMAT deformation. Fig. 2a shows that perfect dislocations are the main defects in grain interior at the position 1, as marked by the yellow arrows. While the density of dislocation is relatively low, leading to slight enhancement of the microhardness. With increasing depth, a significant increase in dislocation density is observed at position 2 (Fig. 2b). Clearly, perfect dislocations still exit at this position. Due to the higher deformation strain, a large number of dislocation tangles are formed in the grain interior. It is well established that SMAT processing can produce an ultra-high strain at the surface. K. Lu et al. reported that a high-strength nanocrystalline grains in pure Cu was produced at the surface layer

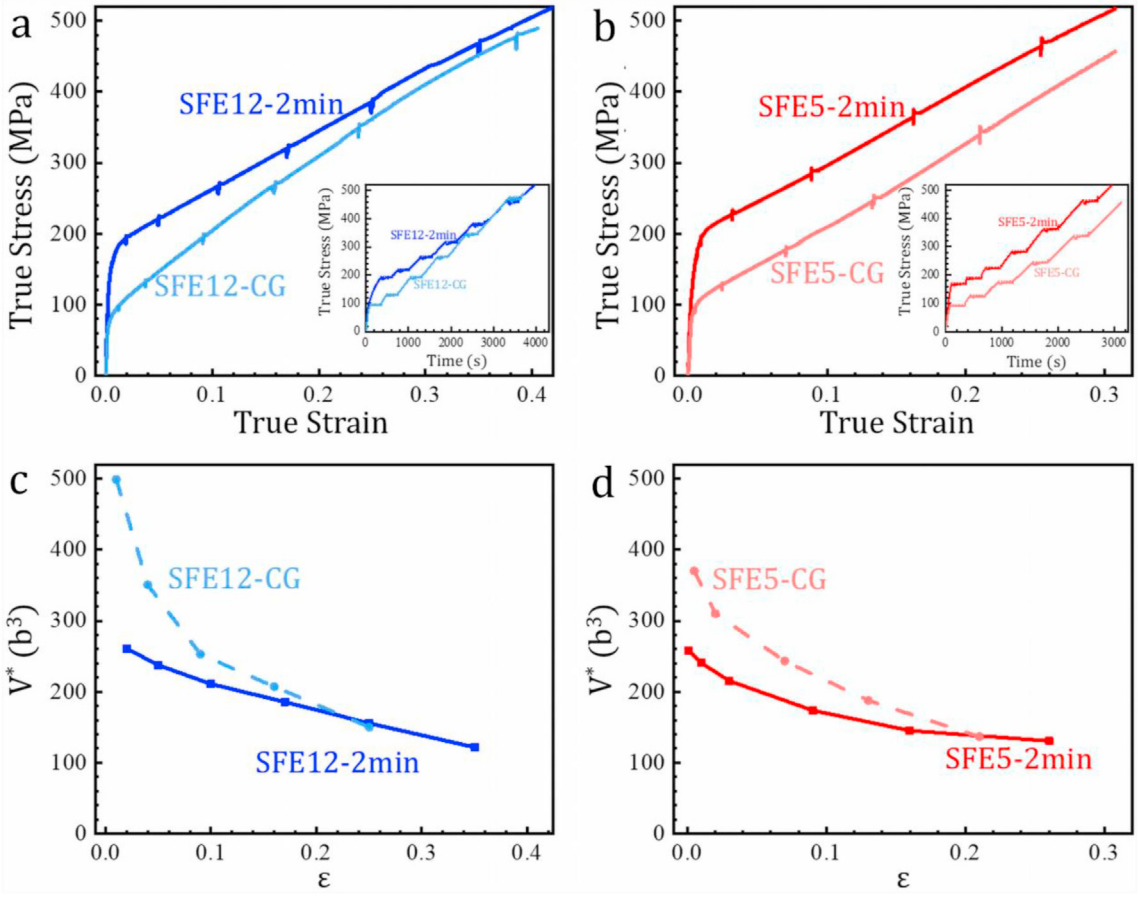

Fig. 4 – Cyclical stress relaxation test of Cu-Al alloys. (a) and (b) true stress-strain curves of SFE 12 and SFE5 alloys, respectively, inserted with true stress-time curves; (c) and (d) physical activation volume V* for different strains of SFE 12 and SFE5 alloys, respectively.

[11,35]. Owing to the extreme low stacking fault energy in the alloys investigated here, high density nano-twins, co-existed with nano stacking faults, are formed nearby the surface layer (Fig. 2c–1). Contribution of nano stacking faults to yield strength was raised by Jian et al. [36]. They proposed that the relationship of yield strength is inversely proportional to the average spacing of stacking faults. According to Hall–Petch equation, the yield strength improved by grain boundaries is inversely proportional to the square root of grain size [32,33,37,38]. Thus, stacking fault are also effective in strengthening, especially due to its ultra-nano space that is difficult to obtain by grain refinement [39]. Fig. 2c–2 shows the high-resolution TEM image in the area of a nano twin. Although, the average thickness of the nano twins is only ~10 nm, the twins provide significant blocking effects on the dislocations slipping in the {111} planes, as marked by the white lines.

The typical tensile stress-strain curves of both the SFE12 and SFE5 samples before and after SMAT are shown in Fig. 3a. Both the alloys show a significant improvement of yield stress, from ~90 MPa to ~170 MPa, as shown in Fig. 3b. The yield strength is increased to more than 1.5 times, due to the pronounced work hardening induced by SMAT process. Interestingly, the uniform elongation remains stable, especially in the SFE5 sample, exhibiting 72.6% vs. 71.3% before and after SMAT deformation (Fig. 3b). This result is different from the long-established theory that work hardening is usually at the expense of ductility in most of the metallic materials. Fig. 3c shows the strain hardening curves of the SFE12 and SFE5 alloys. Clearly, both the strain hardening rates of SFE5 samples exhibit a notable up-turn (from the strain of 0.02–0.2), while is not visible in the SFE12 sample. The up-turn of strain hardening rate keeps a stable deformation and delays the necking of the tensile samples. Thus, the uniform elongation of SMATed SFE5 alloy is much better than that of SFE12 alloy. A single gradient layer with a thickness of about 400 μm can increase the yield strength by nearly 90% for a 4 mm thick bulk material with little loss of ductility, and the potential strain hardening mechanism is worth investigating.

Fig. 4a and b shows the repeated stress relaxations for Cu-Al alloys. The SFE12 sample exhibits less significant stress drop $\Delta\sigma$ in each relaxation cycle than the SFE5 sample. According to the method introduced in Ref. [40], the physical activation volume, V*, can be extracted from consecutive relaxation transients in repeated stress-relaxation texts. We plot the V* of SFE12 and SFE5 alloys in Fig. 4c and d, respectively. Clearly, the initial V* in coarse grained SFE5 alloy (~370 b^3) is much lower than that of SFE12 sample (~500 b^3). With the increasing of true stress, the values of V* in both the alloys are decreased. Previous study revealed that the high-

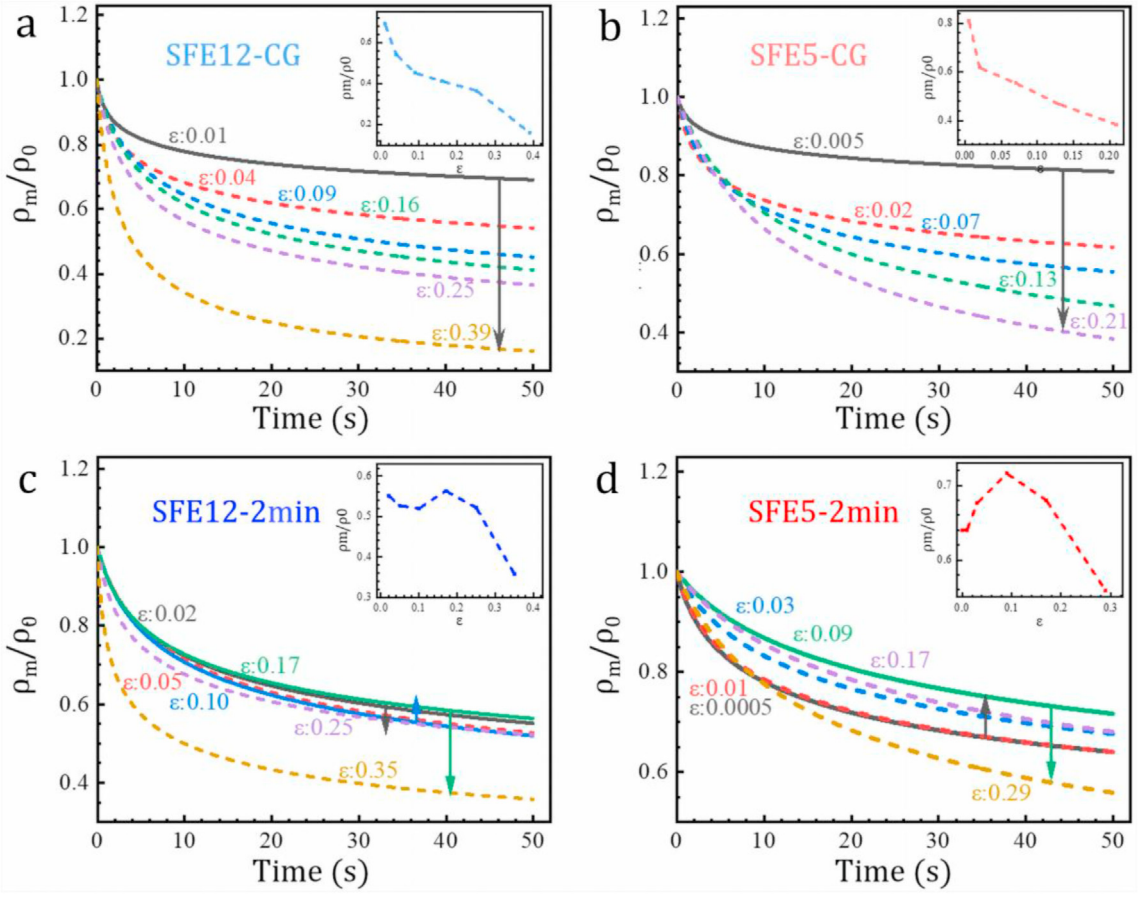

Fig. 5 – Evolution of mobile dislocation density with the third stress relaxation (50s). (a) and (b) SFE12 sample before and after SMAT; (c) and (d) SFE5 samples before and after SMAT. Inset, the value of ρ_m/ρ_0 after relaxation as a function of starting strain.

density twins in ultrafine crystalline copper can effectively reduce dislocation free-range [40]. Owing to the low stacking fault energy in Cu-Al alloy, stacking faults and deformation twins are easy to form with straining. In contrast, the initial V* of SMATed samples are relatively low, SFE12 = 261 b^3 and SFE5 = 258 b^3. Due to the blocking effect by SFs and NTs, the free dislocation swept area is limited in the SMATed samples, thus the initial V* of SMATed samples is much lower than the coarse grained one.

For the plastic flow controlled by thermally activated dislocation glide, the dislocation velocity is given by Ref. [41]:

$$\upsilon = \upsilon_0 \exp\left(\frac{\Delta\tau^* \cdot V^*}{k_B T}\right)$$

where T is the temperature; k_B is the Boltzmann constant; τ^* is the thermal component of the shear stress, υ_0 is the initial dislocation velocity at t = 0, and $\Delta\tau^*$ is the change of τ^* from time t = 0 to time t; $\Delta\tau^* < 0$ indicates a typical stress transient.

It is usually assumed that the mobile dislocation density ρ_m and the dislocation velocity υ are related by an empirical power law:

$$\frac{\rho_m}{\rho_0} = \left(\frac{\upsilon}{\upsilon_0}\right)^{\beta}$$

where β is a dimensionless immobilization parameter, ρ_0 is the dislocation density at the start of the transient.

As shown in Fig. 5a and b, the mobile dislocation density ρ_m/ρ_0 in coarse grained alloys exhibits a continuous reduction with straining. This phenomenon usually occurs in homogeneous materials. In a sharp contrast, the values of ρ_m/ρ_0 show an unexpected increase during the early stage of tensile testing, as shown in Fig. 5c and d. Interestingly, the value of ρ_m/ρ_0 in SMATed SFE5 alloy shows a higher up-turn to more 70% than that of SFE12 alloy. Thus, both the gradient microstructure and low stacking improve the strain-hardening capability of Cu-Al alloy.

As mentioned above, SMAT processing at liquid nitrogen produces a good combination of strength and ductility in Cu-Al alloys, especially in the SFE5 alloy. It has been well established that SFs and NTs are easier to form in the alloys with lower SFE during plastic deformation [42–44]. To investigate the in-depth deformation mechanism, the evolution of GNDs were quantitatively analyzed by EBSD. Based on strain gradient theory [45,46], the distribution of GND is revealed by Eq (3):

$$\rho^{GND} = \frac{2KAM_{ave}}{\mu b} \tag{3}$$

where ρ^{GND} is the density of geometrically necessary dislocations, KAM_{ave} is the average of the kernel average misorientation, μ is the step size of EBSD, and b is the Burgers vector of dislocation.

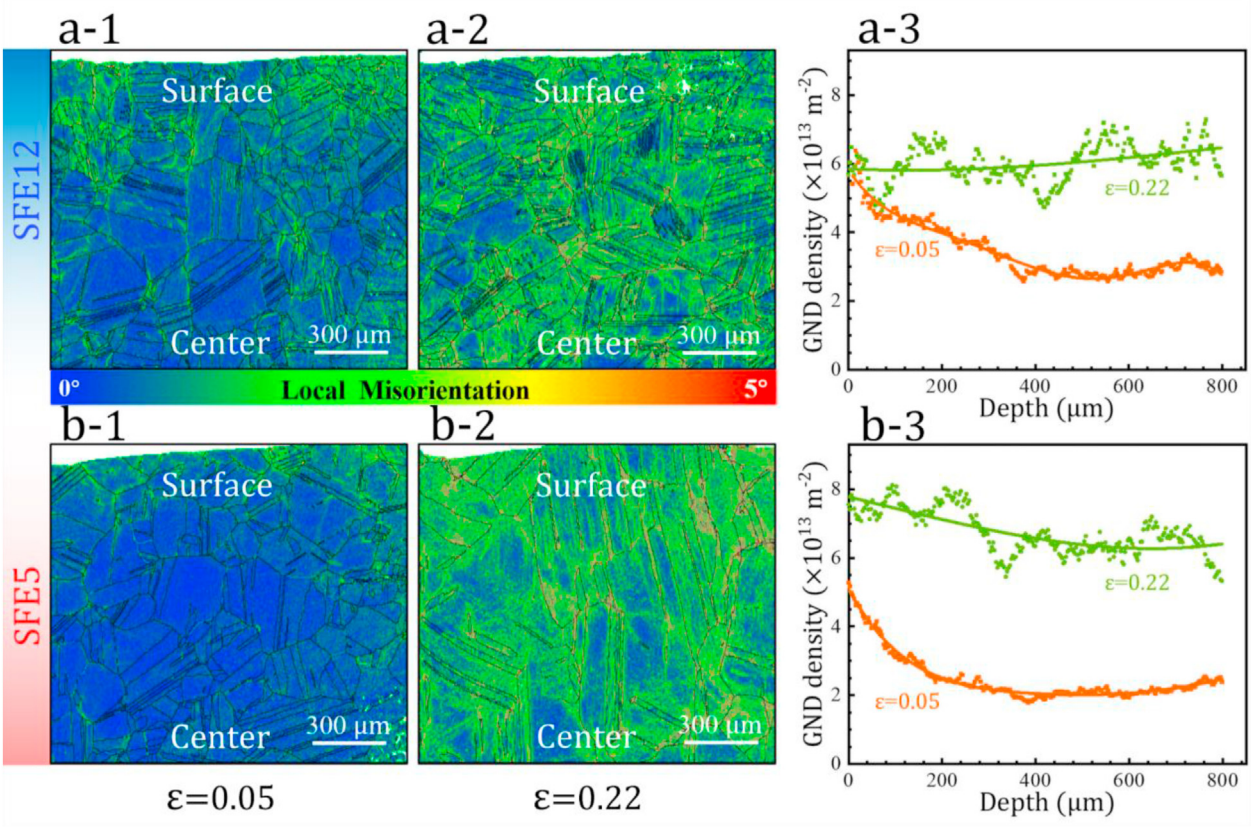

Fig. 6 – EBSD images of Cu-Al alloys with different tensile strain. (a-1) and (a-2) KAM mappings of SFE12 alloy with strains of 0.05 and 0.22; (a-3) distribution of dislocation density with depth in SFE12 alloy; (b-1) and (b-2) KAM mappings of SFE5 alloy with strains of 0.05 and 0.22; (b-3) distribution of dislocation density with depth in SFE5 alloy. The GND density calculated by Eq.(3), and the KAM data were exported from Fig.6a–b by Channel5.

Fig. 6 show the KAM images of the SMATed SFE12 and SFE5 samples with different tensile strains, in which two typical strain of 0.05 and 0.22 are selected for EBSD analysis. At the early stage of deformation ($\varepsilon = 0.05$), both alloys show a gradient distribution of GNDs, which exhibit highest GND density at the surface. As the tensile strain is increased to 0.22, the GND density in the depth of coarse-grained layer is increased significantly (Fig. 6b–1 and b-2). Fig. 6a–3 shows that the GND density at the surface is stable at about 6×10^{13} m^{-2}, which at center (in depth of ~600 μm) is increased from 3×10^{13} m^{-2} to 6×10^{13} m^{-2}. Thus, it is reasonable to imply that highest dislocation density in the SFE12 alloy is near 6×10^{13} m^{-2}. In contrast, the GND' s density at surface of SFE5 is still increased from 5×10^{13} to 8×10^{13} m^{-2} (Fig. 6b–2). The dislocation storage in SFE5 alloy is higher than SFE12 alloy.

Fig. 7 show the bright field TEM images of SFE12 and SFE5 alloys with different tensile strain ($\varepsilon = 0$, 0.05 and 0.22, respectively). Due to the different stacking fault energy, deformation mechanisms of the alloys are not same. As shown in Fig. 7a–1 for the SFE12 sample, the defects in grain interior are dominated by perfect dislocations. A small amount of stacking faults also exist as marked by the pink lines. As the sample is tensile deformed for 0.05 of strain, dislocation tangles as well as the nano twins formed (Fig. 7a–2). Fig. 7a–3 shows a higher strain of 0.22. Clearly, high density of deformation twins with nano size are formed. Thus, the main deformation mechanism in SFE12 alloy is dislocation slipping and twinning. Fig. 7b–1 to b-3 show the microstructure of SFE5 alloy with same deformation strain. The biggest difference is that the density of nano-stacking faults in SFE5 alloy is much higher. As a result, the thickness and density of nano twins formed in SFE5 alloy are much finer and higher than those of in SFE12 alloy. Deformation twins in fcc metals are believed to be formed by the glide of partial dislocations with the same Burgers vector on successive planes [44]. Owing to the lower stacking fault energy, the average thickness of NTs in the SFE5 alloy (5.0 nm) is much smaller than that of in the SFE12 alloy (24.7 nm), as shown in Fig. 7a–4 and b-4.

Fig. 8a shows a high-resolution TEM image of nano twins in SMATed SFE5 alloy from zone axis of [110]. The density of twin is very high, exhibiting an average thickness of ~5.4 nm (Fig. 8b). High density of nano twins have been demonstrated to not only improve the strength efficiently, but also to maintain a good ductility in Cu alloys [33,37,47,48]. As shown in Fig. 8c, nano stacking faults co-exist with nano twins in the SMATed sample. It has been proposed that deformation twins in fcc metals are formed by glide of partial dislocations with the same burgers vector on successive planes. The twinning partial dislocations are all Shockley partials, with a Burgers vector of b = 1/6<112>, which can glide on the slip plane [44]. Thus, lower stacking fault energy introduces more twinning partial dislocations to form nano-twins in SFE5 alloy.

Microstructure evolutions in the SMATed SFE12 and SFE5 alloys are different, owing to their different stacking fault energies. Thus, the mechanical properties, such as straining hardening abilities, are also different during tensile deformation. Fig. 9a and 9b shows the schematic diagram of

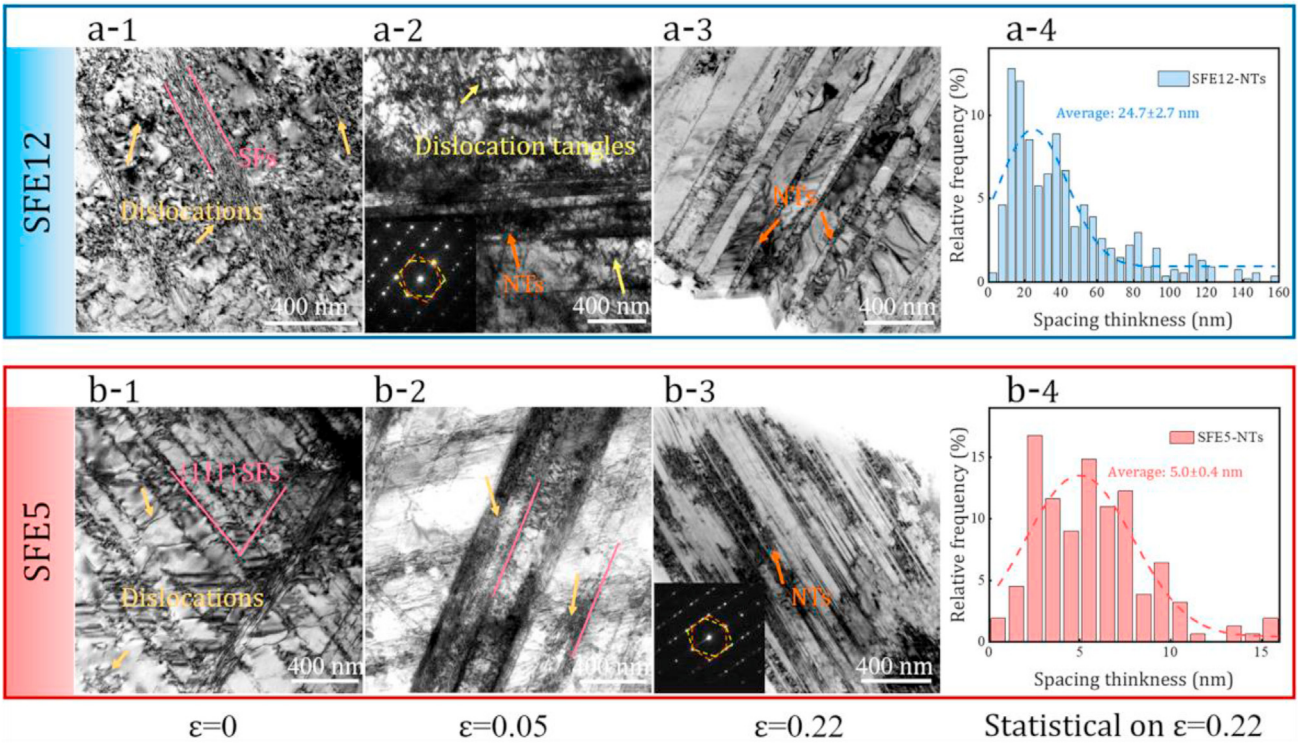

Fig. 7 – Bright-field TEM images of the SMATed Cu-Al alloys at a depth of ~80 μm from surface. (a-1), (a-2) and (a-3) SFE12 sample with $\varepsilon = 0$, 0.05 and 0.22, respectively; (b-1), (b-2) and (b-3) SFE5 sample with $\varepsilon = 0$, 0.05 and 0.22, respectively; (a-4) and (b-4) statistic distribution of twins' thickness in the SFE12 and SFE5 alloys with 0.22 of tensile strain.

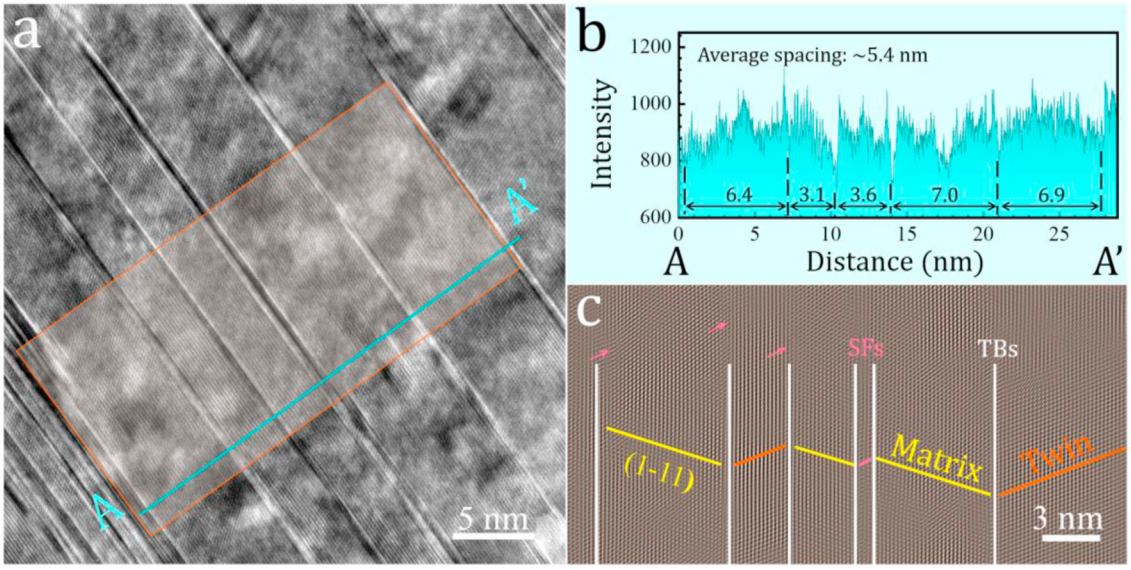

Fig. 8 – Atomic-scaled TEM image of nano twins in 0.22 tensile deformed SFE5 alloy from [110] zone axis. (a) HRTEM image, (b) intensity of nano-twins contrast in (a), (c) close-up atomic microstructure of the brown box in (a).

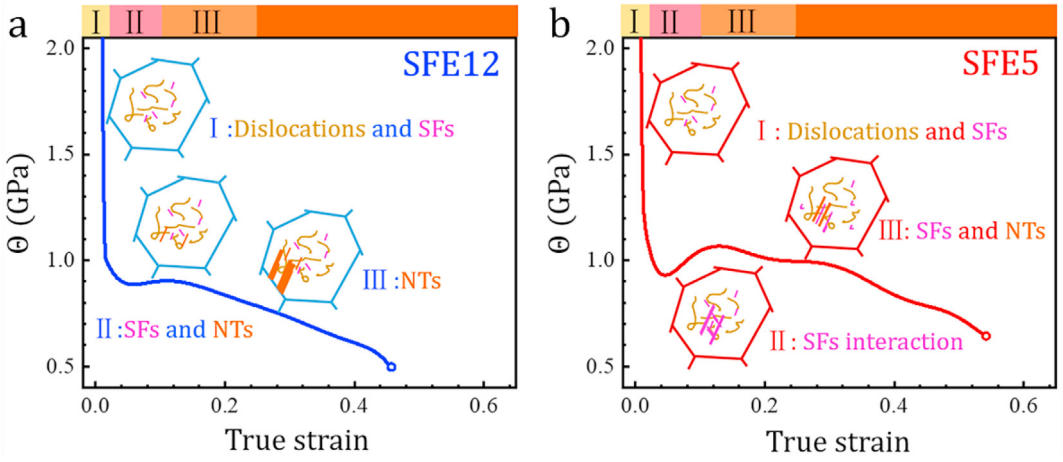

Fig. 9 – Schematic diagram of deformation mechanism of SMATed samples at different stages in work hardening curves. (a) SFE12 alloy; (b) SFE5 alloy.

deformation mechanism of SFE12 and SFE5 alloys, respectively. At the beginning (Stage I) of tension, both the alloys show mixed perfect dislocations and stacking faults in grain interior. In the Stage II, both the stacking faults and nano twins are formed in SFE12 alloy, while nano twin is almost absent in SFE5 alloy. Note that, a significant up-turn of strain-hardening rate happens in this stage, contributing to interaction of high-density stacking faults. In the Stage III, deformation twinning is dominated in the SFE12 alloy. In contrast, stacking faults are still continuous formed in the SFE5 alloy, providing additional strain hardening to delay the necking. As such, reducing the stacking fault energy is considerable for improving the strain hardening of Cu-Al alloys.

4. Conclusions

In this work, two Cu-Al alloys with different stacking fault energies were SMAT processed at liquid nitrogen temperature. The key findings are summarized below:

(1) Nano gradient structured Cu-Al alloys are produced by SMAT processing, leading to a gradient distribution of microhardness form surface to center. There are three typical layers at the depth of 40, 110 and 200 μm, respectively: (i) High density nano-twins and stacking faults co-exist in the layer nearby the surface; (ii) A large number of perfect dislocation entangles formed in the

sub-surface layer; (iii) perfect dislocations dominate in the deformation influenced layer.

(2) The combination of mechanical properties are improved after SMAT. The yield strength of both alloys is improved to more than 1.5 times after SMAT, and the ultimate strength of the samples after SMAT is slightly higher than that of CG samples. While the SFE5 alloy after SMAT exhibits higher ductility than the SFE12 alloy. The strain hardening rate of SFE5 alloy exhibits a notable up-turn during tensile deformation, introducing a more stable deformation to delay the necking.

(3) Low stacking fault energy increase density of nano-stacking faults, leading to finer spacing of nano twins (~5.4 nm) and high dislocation storage (8×10^{13} m^{-2}) in the SMATed SFE5 alloy at the intermediate strain stage. The significant up-turn of strain-hardening rate in SFE5 alloy is also induced by low stacking fault energy.

Declaration of Competing Interest

The authors declare that they have no known competing financial interests or personal relationships that could have appeared to influence the work reported in this paper.

Acknowledgments

This work was supported by the Key Program of National Natural Science Foundation of China (NSFC) (grant number 51931003), and the NSFC (grant numbers 51664033, 52071178), and 2019 JSPS/NSFC Bilateral Joint Research Project (grant number 51911540072). The authors were supported by Basic Research Project of Yunnan Science and Technology Program under Grant No. 202001AU070081.

We thank the technical support from the Jiangsu Key Laboratory of Advanced Micro&Nano Materials and Technology. The SEM and TEM experiments are performed at the Materials Characterization and Research Center of Nanjing University of Science and Technology.

REFERENCES

[1] Gleiter H. Nanocrystalline materials. Prog Mater Sci 1989;33:223–315.
[2] Meyers AMMA, Benson DJ. Hall-Petch strengthening for the microhardness of twelve nanometer grain diameter electrodeposited nickel. Prog Mater Sci 2006;51:427–556.
[3] Koch CC. Structural nanocrystalline materials: an overview. J Mater Sci 2007;42(5):1403–14.
[4] Fang TH, Tao NR, Lu K. Tension-induced softening and hardening in gradient nanograined surface layer in copper. Scripta Mater 2014;77:17–20.
[5] Wei Y, Li Y, Zhu L, Liu Y, Lei X, Wang G, et al. Evading the strength- ductility trade-off dilemma in steel through gradient hierarchical nanotwins. Nat Commun 2014;5(3580).
[6] Guo L, Wu W, Ni S, Yuan Z, Cao Y, Wang Z, et al. Strengthening the FeCoCrNiMo0.15 high entropy alloy by a gradient structure. J Alloys Compd 2020;841.
[7] Wu XL, Jiang P, Chen L, Zhang JF, Yuan FP, Zhu YT. Synergetic strengthening by gradient structure. Materials Research Letters 2014;2(4):185–91.
[8] Shao CW, Zhang P, Zhu YK, Zhang ZJ, Tian YZ, Zhang ZF. Simultaneous improvement of strength and plasticity: additional work-hardening from gradient microstructure. Acta Mater 2018;145:413–28.
[9] Z HW, Liu XC, Lu K. Strain-induced ultrahard and ultrastable nanolaminated structure in nickel. Science 2013;342(6156):337–40.
[10] Pan Q, Zhang L, Feng R, Lu Q, An K, Chuang AC, et al. Gradient-cell–structured high-entropy alloy with exceptional strength and ductility. Science 2021;374(6570):984–9.
[11] Fang TH, Li WL, Tao NR, Lu K. Revealing extraordinary intrinsic tensile plasticity in gradient nano-grained copper. Science 2011;331(6024):1587–90.
[12] Zhu Y, Ameyama K, Anderson PM, Beyerlein IJ, Gao H, Kim HS, et al. Heterostructured materials: superior properties from hetero-zone interaction. Materials Research Letters 2020;9(1):1–31.
[13] Lu L, Wu X, Beyerlein IJ. Preface to the viewpoint set on: heterogeneous gradient and laminated materials. Scripta Mater 2020;187:307–8.
[14] Han SZ, Choi E-A, Lim SH, Kim S, Lee J. Alloy design strategies to increase strength and its trade-offs together. Prog Mater Sci 2020;117:100720.
[15] Huang CX, Wang YF, Ma XL, Yin S, Höppel HW, Göken M, et al. Interface affected zone for optimal strength and ductility in heterogeneous laminate. Mater Today 2018;21(7):713–9.
[16] Wang YF, Huang CX, He Q, Guo FJ, Wang MS, Song LY, et al. Heterostructure induced dispersive shear bands in heterostructured Cu. Scripta Mater 2019;170:76–80.
[17] Zhou H, Huang C, Sha X, Xiao L, Ma X, Höppel HW, et al. In-situ observation of dislocation dynamics near heterostructured interfaces. Materials Research Letters 2019;7(9):376–82.
[18] Wu XL, Jiang P, Chen L, Yuan FP, Zhu YT. Extraordinary strain hardening by gradient structure. Proc Natl Acad Sci U S A 2014;111(20):7197–201.
[19] Wu X, Yang M, Yuan F, Wu G, Wei Y, Huang X, et al. Heterogeneous lamella structure unites ultrafine-grain strength with coarse-grain ductility. Proc Natl Acad Sci U S A 2015;112(47):14501–5.
[20] Lin Y, Pan J, Zhou HF, Gao HJ, Li Y. Mechanical properties and optimal grain size distribution profile of gradient grained nickel. Acta Mater 2018;153:279–89.
[21] Cheng Z, Lu L. The effect of gradient order on mechanical behaviors of gradient nanotwinned Cu. Scripta Mater 2019;164:130–4.
[22] Zhao YH, Zhu YT, Liao XZ, Horita Z, Langdon TG. Tailoring stacking fault energy for high ductility and high strength in ultrafine grained Cu and its alloy. Appl Phys Lett 2006;89(12).
[23] Rohatgi Aashish, Vecchio Kenneth S, Gary George T. The influence of stacking fault energy on the mechanical behavior of Cu and Cu-Al alloys: deformation twinning, work hardening, and dynamic recovery. Metall Mater Trans 2001;32:135–45.
[24] Qu S, An XH, Yang HJ, Huang CX, Yang G, Zang QS, et al. Microstructural evolution and mechanical properties of Cu-Al alloys subjected to equal channel angular pressing. Acta Mater 2009;57(5):1586–601.
[25] Hamdi F, Asgari S. Influence of stacking fault energy and short-range ordering on dynamic recovery and work hardening behavior of copper alloys. Scripta Mater 2010;62(9):693–6.

[26] An XH, Lin QY, Wu SD, Zhang ZF, Figueiredo RB, Gao N, et al. The influence of stacking fault energy on the mechanical properties of nanostructured Cu and Cu-Al alloys processed by high-pressure torsion. Scripta Mater 2011;64(10):954–7.
[27] An XH, Wu SD, Zhang ZF, Figueiredo RB, Gao N, Langdon TG. Enhanced strength-ductility synergy in nanostructured Cu and Cu-Al alloys processed by high-pressure torsion and subsequent annealing. Scripta Mater 2012;66(5):227–30.
[28] Tian YZ, Zhao LJ, Chen S, Terada D, Shibata A, Tsuji N. Optimizing strength and ductility in Cu-Al alloy with recrystallized nanostructures formed by simple cold rolling and annealing. J Mater Sci 2014;49(19):6629–39.
[29] Wang YB, Liao XZ, Zhao YH, Lavernia EJ, Ringer SP, Horita Z, et al. The role of stacking faults and twin boundaries in grain refinement of a Cu–Zn alloy processed by high-pressure torsion. Mater Sci Eng, A 2010;527(18–19):4959–66.
[30] An XH, Lin QY, Wu SD, Zhang ZF, Figueiredo RB, Gao N, et al. Significance of stacking fault energy on microstructural evolution in Cu and Cu–Al alloys processed by high-pressure torsion. Phil Mag 2011;91(25):3307–26.
[31] Liu R, Zhang ZJ, Li LL, An XH, Zhang ZF. Microscopic mechanisms contributing to the synchronous improvement of strength and plasticity (SISP) for TWIP copper alloys. Sci Rep 2015;5:9550.
[32] El-Danaf EA, Soliman MS, Al-Mutlaq AA. Correlation of grain size, stacking fault energy, and texture in Cu-Al alloys deformed under simulated rolling conditions. Adv Mater Sci Eng 2015;2015:1–12.
[33] Tian YZ, Zhao LJ, Park N, Liu R, Zhang P, Zhang ZJ, et al. Revealing the deformation mechanisms of Cu–Al alloys with high strength and good ductility. Acta Mater 2016;110:61–72.
[34] J.P.V. M. F. DENANOT The stacking fault energy in Cu-Al-Zn alloys. phys. stat. sol. a 1971;(8):K125–7.
[35] Lu K. Nanomaterials. Making strong nanomaterials ductile with gradients. Science 2014;345(6203):1455–6.
[36] Jian WW, Cheng GM, Xu WZ, Yuan H, Tsai MH, Wang QD, et al. Ultrastrong Mg alloy via nano-spaced stacking faults. Materials Research Letters 2013;1(2):61–6.
[37] Tian YZ, Zhao LJ, Chen S, Shibata A, Zhang ZF, Tsuji N. Significant contribution of stacking faults to the strain hardening behavior of Cu-15%Al alloy with different grain sizes. Sci Rep 2015;5:16707.
[38] Zhou X, Li X, Lu K. Size dependence of grain boundary migration in metals under mechanical loading. Phys Rev Lett 2019;122(12):126101.
[39] Wei K, Hu R, Yin D, Xiao L, Pang S, Cao Y, et al. Grain size effect on tensile properties and slip systems of pure magnesium. Acta Mater 2021;206.
[40] Lu L, Zhu T, Shen Y, Dao M, Lu K, Suresh S. Stress relaxation and the structure size-dependence of plastic deformation in nanotwinned copper. Acta Mater 2009;57(17):5165–73.
[41] Caillard D, Martin JL. Thermally activated mechanisms in crystal plasticity, vol. 8; 2003. p. 3–433.
[42] Zhu YT, Langdon TG. Influence of grain size on deformation mechanisms: an extension to nanocrystalline materials. Mater Sci Eng, A 2005;409(1–2):234–42.
[43] Zhu YT, Narayan J, Hirth JP, Mahajan S, Wu XL, Liao XZ. Formation of single and multiple deformation twins in nanocrystalline fcc metals. Acta Mater 2009;57(13):3763–70.
[44] Zhu YT, Liao XZ, Wu XL. Deformation twinning in nanocrystalline materials. Prog Mater Sci 2012;57(1):1–62.
[45] Gao YHH, Nix WD. Mechanism based strain gradient plasticity-I. Theory. J Mech Phys Solid 1999;47:1239–63.
[46] Kubin AMLP. Geometrically necessary dislocations and strain-gradient plasticity:a few critical issues. Scripta Mater 2003;48:119–25.
[47] Chen W, You ZS, Tao NR, Jin ZH, Lu L. Mechanically-induced grain coarsening in gradient nano-grained copper. Acta Mater 2017;125:255–64.
[48] Wang JJ, Tao NR, Lu K. Revealing the deformation mechanisms of nanograins in gradient nanostructured Cu and CuAl alloys under tension. Acta Mater 2019;180:231–42.